Multichannel Topological Kondo Effect

Guangjie Li,[1] Yuval Oreg,[2] and Jukka I. Väyrynen[1,3]

[1]*Department of Physics and Astronomy, Purdue University, West Lafayette, Indiana 47907, USA*
[2]*Department of Condensed Matter Physics, Weizmann Institute of Science, Rehovot 76100, Israel*
[3]*Purdue Quantum Science and Engineering Institute, Purdue University, West Lafayette, Indiana 47907, USA*

(Received 27 July 2022; revised 10 November 2022; accepted 11 January 2023; published 10 February 2023)

A Coulomb blockaded M-Majorana island coupled to normal metal leads realizes a novel type of Kondo effect where the effective impurity "spin" transforms under the orthogonal group $\mathrm{SO}(M)$. The impurity spin stems from the nonlocal topological ground state degeneracy of the island and thus the effect is known as the topological Kondo effect. We introduce a physically motivated N-channel generalization of the topological Kondo model. Starting from the simplest case $N=2$, we conjecture a stable intermediate coupling fixed point and evaluate the resulting low-temperature impurity entropy. The impurity entropy indicates that an emergent Fibonacci anyon can be realized in the $N=2$ model. We also map the case $N=2$, $M=4$ to the conventional four-channel Kondo model and find the conductance at the intermediate fixed point. By using the perturbative renormalization group, we also analyze the large-N limit, where the fixed point moves to weak coupling. In the isotropic limit, we find an intermediate stable fixed point, which is stable to "exchange" coupling anisotropies, but unstable to channel anisotropy. We evaluate the fixed point impurity entropy and conductance to obtain experimentally observable signatures of our results. In the large-N limit, we evaluate the full crossover function describing the temperature-dependent conductance.

DOI: 10.1103/PhysRevLett.130.066302

Introduction.—Since the original Kondo model of a magnetic impurity screened by a single orbital in a metal [1], its multichannel generalization [2], especially in mesoscopic devices [3,4], has proven to be a fruitful system exemplifying exotic many-body phenomena [5–10], such as emergent anyonic excitations [11–14], even in the simplest two-channel Kondo (2CK) model [15,16]. The key parameters that determine the behavior of the system are the spin of the impurity (S) and the largest possible total spin ($N/2$) for N channels of conduction electrons. When $N > 2S$, namely, the overscreened case [2], the low-temperature fixed point is at intermediate coupling strength, with both weak and strong coupling fixed points unstable. Notably, in the limit of large N, the intermediate coupling fixed point moves toward weak coupling and becomes perturbatively accessible in $1/N$ expansion [2,17].

The intermediate coupling fixed point cannot generically be described by a Fermi liquid theory. For example, in a mesoscopic 2CK device, the conductance correction near $T=0$ is proportional to T [7,9], and not to T^2 expected of a Fermi liquid [18]. Besides the conductance, the impurity entropy also shows exotic noninteger quantum dimension, which can be interpreted as a fractional ground state degeneracy. As shown by Emery and Kivelson [15] (see also Refs. [16,19,20]), an emergent Majorana will remain of the impurity spin after the screening by conduction electrons. The low-temperature impurity entropy is given by $\ln\sqrt{2}$, where $\sqrt{2}$ is the quantum dimension of a single Majorana (two uncoupled Majoranas have a ground state degeneracy 2). For a 3CK model, the screened impurity entropy is $\ln\varphi$, where $\varphi = (1+\sqrt{5})/2$ is the Golden ratio [21,22], exhibiting the quantum dimension of a Fibonacci anyon. The conventional multichannel Kondo (MCK) models based on the SU(2) symmetry group (which is natural in the case of a magnetic impurity) have been extensively studied by using conformal field theory (CFT) [5,23–30] and various other methods [17,31–40].

It is natural to expect that the rich physics of the multichannel Kondo effect can be further expanded by considering symmetry groups beyond the conventional SU(2). Recently, Béri and Cooper [41,42] showed that a Coulomb blockaded topological superconductor hosting M-Majorana zero modes coupled to M normal metal leads displays a Kondo interaction with $\mathrm{SO}(M)$ symmetry [43]. Even though this "topological Kondo" model has only one $\mathrm{SO}(M)$ channel [46], in certain cases (such as $M=3,4$) it can be mapped to an SU(2) MCK model and therefore has non-Fermi liquid (NFL) behavior at low temperatures. For example, the conductance correction near $T=0$ is proportional to $T^{2(M-2)/M}$ and the impurity entropy generically indicates a fractional ground state degeneracy [48]. With the $\mathrm{SO}(M)$ symmetry group providing a relatively stable NFL fixed point, the single-channel topological Kondo model has attracted a wide range of detailed studies and extensions [49–60]. However, the multichannel version of it has not yet been studied.

In this Letter, we generalize the topological Kondo model to $N \geq 2$ channels and propose a physical realization for it. Already in the relatively simple $N = 2$, $M = 8$ case we find a quantum dimension indicating an emergent Fibonacci anyon, which cannot be realized for any M in the single channel SO(M) model. In this simplest two-channel generalization, we also find a mapping between SO(4) and a conventional 4CK model, allowing us to find the exact fractional fixed point conductance, Eq. (2). In order to study a more general case, we then introduce large-N perturbation theory similar to what has been done with the SU(2) case [36,61,62]. We focus on the experimentally relevant observables of the conductance [7,9,63] and impurity entropy [22,64–68].

Two-channel topological Kondo model.—The two-channel generalization of the isotropic topological Kondo interaction Hamiltonian is

$$H_K = \lambda_1 \boldsymbol{S} \cdot \boldsymbol{J}_1(x_0) + \lambda_2 \boldsymbol{S} \cdot \boldsymbol{J}_2(x_0), \tag{1}$$

where $S^{(\alpha,\beta)} = -\mathrm{i}\gamma_\alpha\gamma_\beta/2$ and $J_i^{(\alpha,\beta)} = -\mathrm{i}(\psi_{i,\alpha}^\dagger \psi_{i,\beta} - \psi_{i,\beta}^\dagger \psi_{i,\alpha})$ are, respectively, the impurity and conduction electron spin operators that satisfy the SO(M) algebra; the vectors $\boldsymbol{S}$ and $\boldsymbol{J}$ are formed of $M(M-1)/2$ components labeled by (α, β) with $\alpha \neq \beta$ taking values from 1 to M.

The interaction (1) arises from a tunneling Hamiltonian $\sum_{i,\alpha} t_\alpha^i \gamma_\alpha \psi_{i,\alpha}^\dagger(x_0) + \mathrm{H.c.}$ between the normal metal leads (fermion operators $\psi_{i,\alpha}$) and the Coulomb blockaded Majorana island (Majorana operators γ_α) with tunneling amplitudes t_α^i (which for simplicity we take to be real) and can be realized in the setup depicted in Fig. 1(a). We connect each Majorana of the island to two leads, labeled $i = 1, 2$, which we call "channels." The M subchannels in each channel (which is also the number of Majoranas) are dubbed different "flavors," labeled by α. In order to prevent tunneling from mixing different channels, we have added a charging energy E_{c_2} for the second channel. Thus, the $i = 2$

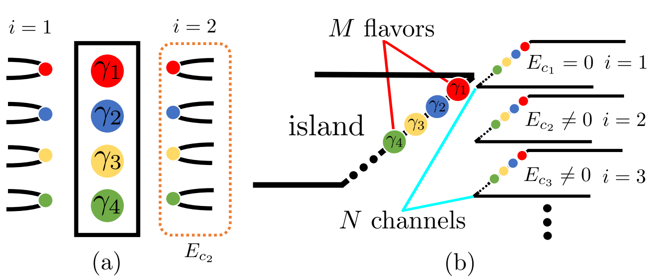

FIG. 1. (a) $N = 2$ SO(4) topological Kondo model. The box at the middle is the Majorana island and the wires (leads) at the left and right hold conduction electrons. Each wire inside a channel is connected to a Majorana zero mode (labeled by $\gamma_{1,2,3,4}$) in the island. (b) N-channel SO(M) topological Kondo model. The number of Majorana zero modes (flavors) is M and the number of layers (channels) is N. The charging energy E_{c_i} (E_{c_1} is zero and all others are nonzero) is essential for each channel to prevent channel mixing.

"lead" should be considered as a large quantum dot with small level spacing but significant charging energy in full analogy with the proposal of Ref. [63], used to implement the 2CK effect in quantum dots. In the weak-tunneling limit, the effective exchange interaction strength is then $\lambda_{i,\alpha\beta} \propto t_\alpha^i t_\beta^i / U_i$, where U_i is the charging energy.

We will first focus on a two-channel SO(4) topological Kondo model, which can be exactly mapped to a 4CK model. The reason is that we can consider SO($M = 4$) as two independent "spins," i.e., $\mathrm{SO}(4) \sim \mathrm{SU}(2) \times \mathrm{SU}(2)$, which allows us to unitarily transform $\psi_{i,\alpha}$ (with channel index $i = 1, 2$ and flavor index $\alpha = 1, 2, 3, 4$) to $\psi_{n,\sigma}(n = 1, 2, 3, 4; \sigma = \uparrow, \downarrow)$ (see Supplemental Material [69]). Likewise, with the total charge of the Majorana island fixed, one can form a single SU(2) spin 1/2 out of the four Majorana operators γ_α. Thus, we have an overscreened Kondo problem that makes the strong coupling fixed point unstable [2] and we expect a stable intermediate coupling fixed point in the isotropic case, where we take $\lambda_1 = \lambda_2$ in Eq. (1).

Overscreening implies the NFL behavior. In order to probe the NFL nature of this low-temperature fixed point, one can measure the fixed point conductance at $T = 0$. Because of the charging energy of other channels, except the channel $i = 1$, we define the conductance matrix [50] $G_{\alpha,\beta}$ in the first channel as the charge current in (flavor) lead α as a linear response to weak voltage $V_\beta \to 0$ applied to lead β, i.e., $G_{\alpha,\beta} = \langle I_\alpha \rangle / V_\beta$. We expect a nonzero fixed point conductance and the corresponding correction to conductance near $T = 0$ will be $T^{(M-2)/(M+2)}$ based on our large-N results and the scaling dimension of the leading irrelevant operator in the CFT [21,24–26], see discussion below Eq. (8). For example, when $N = 2$ and $M = 4$, we expect

$$G_{\alpha \neq \beta}(T) = \frac{e^2}{4h} \left[1 + c_{\alpha\beta} \left(\frac{T}{T_K} \right)^{1/3} \right]. \tag{2}$$

The dimensionless coefficients $c_{\alpha\beta}$ (of order one) and the Kondo temperature T_K are not predicted by the CFT method. We used the fact that the two-channel SO(4) topological Kondo model can be mapped to the 4CK model after fixing the parity [69], see also Eq. (9). The nontrivial fractional power of the temperature dependence signifies the NFL behavior at low temperatures.

Another observable that also shows NFL behavior is the impurity entropy at the fixed point. It is given by $S_{\mathrm{imp}} = \ln g$, where g is usually interpreted as ground state degeneracy. The $N = 1$ topological Kondo model was shown to have $g = \sqrt{M}$ for odd M and $g = \sqrt{M/2}$ for even M by Altland *et al.* [48]. Even though the one-channel impurity entropy shows a nontrivial result, the $N = 2$ case is even more complex,

$$g = \begin{cases} \frac{1}{2}\sqrt{M+2}/\cos[\frac{\pi M}{2(M+2)}], & M \text{ is odd}, \\ \frac{1}{2}\sqrt{(M+2)/2}/\cos[\frac{\pi M}{2(M+2)}], & M \text{ is even}. \end{cases} \tag{3}$$

Again, the impurity entropy of a two-channel SO(4) topological Kondo model from Eq. (3) is $\ln\sqrt{3}$, which is the same as the impurity entropy of a 4CK model [5,21,70] and exhibits the quantum dimension $\sqrt{3}$ of a Z_3 parafermion [71]. Interestingly, two-channel SO(8) has $g = 2 + \varphi$, which indicates an emergent Fibonacci anyon (similar to the 3CK effect). Both of the above two observables at this fixed point show fractional values, which are beyond Fermi liquid description and indicate emergent anyonic excitations. We point out that, for a fixed M, the impurity entropy and g are larger in the two-channel case as compared to $N = 1$. Indeed, g approaches monotonically the degeneracy of M free Majoranas in the large-N limit, see Eq. (10) below.

The charging energy E_{c_2} is essential for the multichannel topological Kondo model. Otherwise, when $E_{c_2} = 0$, the interaction couples only to a single effective channel with a fermion operator $\tilde{\psi}_\alpha(x_0) = \sum_i (t^i_\alpha/|\vec{t}_\alpha|)\psi_{i,\alpha}(x_0)$ and reduces to the conventional $N = 1$ topological Kondo Hamiltonian; When $E_{c_2} \neq 0$ with fine-tuned $\lambda_1 = \lambda_2$, we will have an intermediate coupling fixed point. In the case $\lambda_1 \neq \lambda_2$, based on our large-N calculations discussed below, we expect that the weaker coupling renormalizes to zero and the single-channel limit is recovered.

$N \gg 1$*: Layered construction.*—Next, we generalize the Hamiltonian (1) to N channels. Without exchange isotropy, the interaction becomes

$$H_K = \sum_{i=1}^{N} \sum_{\alpha<\beta=2}^{M} \lambda_{i,\alpha\beta} S^{(\alpha,\beta)} J_i^{(\alpha,\beta)}(x_0). \tag{4}$$

The coupling constant $\lambda_{i,\alpha\beta}$ is real with symmetry $\lambda_{i,\alpha\beta} = \lambda_{i,\beta\alpha}$, which makes Eq. (4) Hermitian. A physical realization for this N-channel model can be implemented by using a layered structure depicted in Fig. 1(b), where each layer with M flavors encodes a single SO(M) channel. Here, channel mixing is prevented by a charging energy E_{c_i} of each channel (except $i = 1$) [63]. Therefore, E_{c_i} needs to be larger than the temperature or bias voltage (however, large E_{c_i} will decrease the bare Kondo couplings $\lambda_{i,\alpha\beta}$). When $E_{c_i} \neq 0$ with λ independent of both channel and flavor indices, we will have an intermediate fixed point at weak coupling, which is found to be stable in terms of anisotropy of flavors; without fine-tuning of channel couplings, the weaker channel couplings flow to zero, considering large N.

By using the perturbative renormalization group (RG) in the large-N limit [17,36,61,72,73], we derive the third-order equation for the coupling constant $\lambda_{i,\alpha\beta}$ from Eq. (4),

$$\frac{d\lambda_{i,\alpha\beta}}{dl} = \rho_0(\lambda_i^2)_{\alpha\beta} - \rho_0^2\lambda_{i,\alpha\beta}\sum_j[(\lambda_j^2)_{\alpha\alpha} + (\lambda_j^2)_{\beta\beta} - 2(\lambda_{j,\alpha\beta})^2], \tag{5}$$

where $l = \ln(D_0/D)$, with $D(D_0)$ denoting the running (bare) cutoff energy scale, and ρ_0 is the density of states per length. The three third-order terms in Eq. (5) correspond to the three Feynman diagrams in Fig. 2(a). On the isotropic line $\lambda_{i,\alpha\beta} = \lambda$ (for $\alpha \neq \beta$), we have

$$\frac{d\lambda}{dl} = (M-2)(1 - 2N\rho_0\lambda)\rho_0\lambda^2. \tag{6}$$

Thus, the stable intermediate fixed point is $\lambda_* = 1/(2N\rho_0)$ and moves to weak coupling in the large-N limit. At $\lambda \approx \lambda_*$, $(d\lambda/dl) \equiv \beta(\lambda) \approx -(M-2)(\lambda - \lambda_*)/(2N)$. The slope of the beta function is $\beta'(\lambda_*) = -(M-2)/(2N)$ which means a large-N scaling dimension $1 + (M-2)/(2N)$ in the irrelevant direction. This agrees with the scaling dimension of the leading irrelevant operator (LIO) with N channels and M flavors $\Delta_{\text{LIO}} = 1 + (M-2)/(2N + M - 2)$ obtained from the CFT [21,24–26,74,75]. The fourth- and fifth-order corrections to Eq. (6) are, respectively, of order $NM^2\rho_0^3\lambda^4$ and $N^2M^2\rho_0^4\lambda^5$ and are subleading by a factor M/N, which makes the large-N perturbation expansion convergent [41,61].

The solution of Eq. (6) is

$$\frac{\lambda(D)}{\lambda_*} = f^{-1}\left[\frac{(D/T_K)^\Delta}{e^2}\right], \qquad f(x) = |1/x - 1|e^{1/x-1}, \tag{7}$$

where we introduced the Kondo temperature $T_K = D_0[e^2 f(\lambda_0/\lambda_*)]^{-1/\Delta}$ and $\Delta = (M-2)/(2N)$. We will have two solutions for Eq. (7) depending on whether the initial

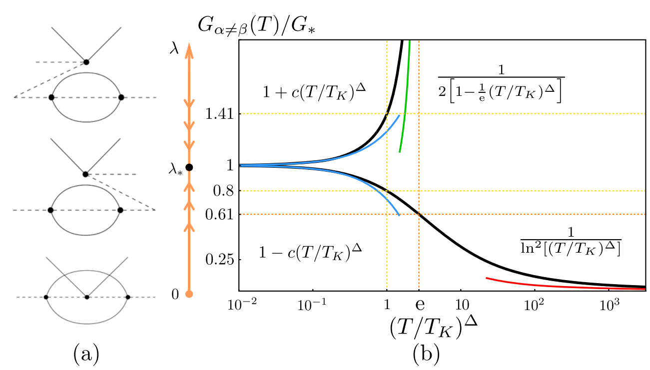

FIG. 2. (a) The leading Feynman diagrams contributing to the third-order RG equation [Eq. (5)] in the large-N limit. The solid lines denote fermions and dashed lines denote Majorana operators. (b) Left: RG flow of the isotropic Kondo exchange coupling with a stable fixed point λ_* (black point). Right: the conductance vs the temperature for two initial conditions $\lambda_0 \lessgtr \lambda_*$ in the large-N limit. When $\lambda_0 < \lambda_*$, the conductance ratio $G(T)/G_*$ is given by the lower black line with a high-temperature approximation $1/\ln^2[(T/T_K)^\Delta]$ (red line), while at low temperature $G(T)/G_* \approx 1 - c(T/T_K)^\Delta$ (lower blue line), with $c = 2/e^2 \approx 0.27$. Here, $G_* = (e^2/h)(\pi^2/4N^2)$ is the conductance at the fixed point λ_*, see Eq. (8). When $\lambda_0 > \lambda_*$, we have $G(T)/G_* \approx 1 + c(T/T_K)^\Delta$ at low temperature (upper blue line), while at high temperature G diverges as $G(T)/G_* \approx 1/[2 - 2(D/T_K)^\Delta/e]$ (green line) at $(T/T_K)^\Delta = e$, signifying breakdown of the weak coupling perturbation theory.

(bare) coupling constant $\lambda_0 = \lambda(D_0)$ is larger or smaller than the fixed point coupling λ_* [see Fig. 2(b)]. Since the low-energy fixed point is at weak coupling in the large-N limit, Eq. (7) gives the full crossover for the running coupling $\lambda(D)$, extending beyond the CFT prediction.

Conductance at large N.—In both $N = 1$, SO(M) topological Kondo model [41,42,49,50,52] and $N = 2$, SO(4) topological Kondo model [Eq. (2)], the fixed point ($T = 0$) conductance is given by a universal fractional multiple of $G_0 = e^2/h$. Here, we first evaluate the conductance perturbatively in λ_0 by using the Kubo formula [69] and find $G_{\alpha\beta} = G_0(\pi\lambda_0\rho_0)^2(1 - M\delta_{\alpha\beta})$ to lowest order. By evaluating the next-order correction to the conductance at finite frequency ω, we find a logarithmic divergence $\sim\lambda_0^3 \ln(D/D_0)$, where $D = \max\{T, \omega\}$. The divergence results from renormalization of the coupling λ, described by the RG equation (6). This indicates that for $T \gg \omega$, $G_{\alpha\neq\beta}(T) = G_0[\pi\lambda(T)\rho_0]^2$, plotted as a function of temperature in Fig. 2(b). Remarkably, in the large-N limit, $\lambda(T)$ remains small and the full crossover function (7) can be found exactly as long as the bare coupling λ_0 is small. At low temperatures, $T \ll T_K$, the conductance approaches its zero-temperature value with a power-law characteristic of a NFL,

$$G_{\alpha\neq\beta}(T)/G_0 = \frac{\pi^2}{4N^2}\left[1 + c_{\alpha\beta}\left(\frac{T}{T_K}\right)^{(M-2)/2N}\right], \quad (8)$$

where the dimensionless constant can be explicitly obtained in the isotropic case, $c_{\alpha\beta} = \pm\delta_{\alpha,\beta}c$ with $c = (2/e^2) \approx 0.27$, based on the crossover function (7). (The sign $\pm$ is determined by the initial condition $\lambda_0 \gtrless \lambda_*$.) The temperature-dependent correction $\sim T^{\Delta_{\rm LIO}-1}$, also obtained from Eq. (7), matches with first-order correction from the leading irrelevant operator, see below Eq. (6), somewhat similar to the case of resistivity in an SU(2) MCK model [27]. This is notably different from the single-channel topological Kondo effect where the first-order correction vanishes [41] and temperature correction is $\sim T^{2(\Delta_{\rm LIO}-1)}$.

The fixed point ($T = 0$) conductance above (i.e., the first term) can be verified for $M = 4$, in which case we can map the N-channel SO(4) topological Kondo model to 2NCK by a unitary transformation (see Supplemental Material [69]). From the mapping, we find the conductance of the N-channel SO(4) model [69],

$$G_{\alpha\neq\beta}(M = 4, T = 0)/G_0 = \sin^2[\pi/(2N + 2)], \quad (9)$$

which bears resemblance to the 2NCK fixed point conductance [31,32]. The $N = 2$ case gives the fixed point conductance (first term) in Eq. (2). The $N = 1$ result agrees with Refs. [42,49,50], whereas the large-N limit agrees with our previous result, Eq. (8).

Impurity entropy at large N.—The NFL nature of the low-temperature fixed point becomes apparent in the impurity entropy $S_{\rm imp} = \ln g$, where g can take a noninteger value. As mentioned in the Introduction and displayed by Eq. (3), the one- and two-channel topological Kondo models generically show a noninteger g. Also, g for the N-channel case can be calculated by using a modular S matrix [21,30]. The modular S matrix of SO(M) is given in Ref. [76] and the general information of it can also be found in Ref. [77]. We then find Eq. (3) in the case $N = 2$. Above we saw that in the large-N limit the fixed point coupling moves to weak coupling. In this case, the impurity is weakly screened and we find in the large-N limit,

$$g = \begin{cases} 2^{(M-1)/2}\left[1 - \frac{(M-2)(M-1)M\pi^2}{192N^2}\right], & M \text{ is odd}, \\ 2^{(M-2)/2}\left[1 - \frac{(M-2)(M-1)M\pi^2}{192N^2}\right], & M \text{ is even}. \end{cases} \quad (10)$$

This result indeed reflects the fact that the impurity is almost free at large N [the same conclusion can be made from the conductance (8)]. The impurity entropy is that of M free Majoranas (with a fixed total parity) with a correction of order $1/N^2$ from the screening by the itinerant electrons. The values in Eq. (3) are the ground state degeneracy at the fixed point λ_* without taking the large-N limit. They are smaller than the above first term, giving the ground state degeneracy at $\lambda = 0$. This agrees with the g theorem in CFT, stating that the ground state degeneracy becomes smaller along the RG flow [23,27,70,78] from $\lambda = 0$ to λ_*.

Flavor anisotropy.—Since the NFL behavior in the conventional single-channel topological Kondo model is stable to flavor anisotropy [41], it is natural to expect the same to be true for its multichannel generalization. Indeed, by considering the physically motivated [69] flavor-anisotropic coupling $\lambda_{\alpha\beta} = [\lambda + (\lambda' - \lambda)(\delta_{1\alpha} + \delta_{1\beta})]$ in Eq. (5), we find two nontrivial fixed points with the majority coupling $\lambda = 1/(2N\rho_0)$ in both, while the minority coupling is either $\lambda' = 1/(2N\rho_0)$ or $\lambda' = 0$. The first one is isotropic and stable, while the second fixed point is unstable, see Fig. 3(a). Thus, flavor anisotropy remains irrelevant in the multichannel generalization of the topological Kondo model.

Channel anisotropy.—Since the NFL fixed point of the conventional SU(2) MCK model is unstable to channel anisotropy [2,74,79], it is crucial to investigate channel anisotropy in the multichannel topological Kondo model. We consider a flavor isotropic but channel anisotropic version of Eq. (4) with $\lambda_{i,\alpha\beta} = \lambda_1$ for $i = 1, \ldots, N_1$ and $\lambda_{N_1+i,\alpha\beta} = \lambda_2$ for $i = 1, \ldots, N_2$. If we consider large-N_1 and large-N_2 limits, we will have ($j = 1, 2$)

$$\frac{d\lambda_j}{dl} = (M - 2)\lambda_j\rho_0(\lambda_j - 2N_1\lambda_1^2\rho_0 - 2N_2\lambda_2^2\rho_0). \quad (11)$$

The RG flow is shown in Fig. 3(b) and has two stable anisotropic fixed points. When $\lambda_1 \neq \lambda_2$, the smaller coupling constant flows to zero and the larger one λ_i flows to

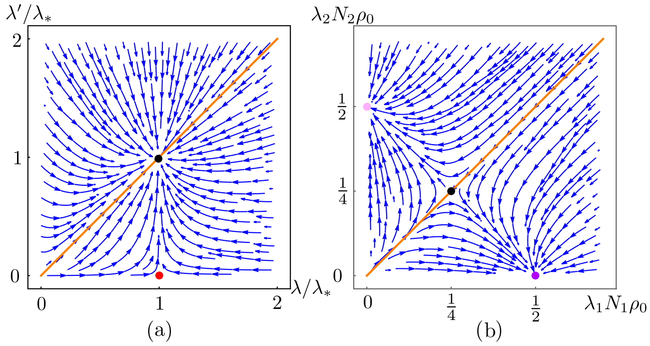

FIG. 3. RG flow of (a) flavor and (b) channel anisotropies. The isotropic lines are denoted in orange with the black point showing the isotropic intermediate fixed point. (a) Flavor anisotropy. The isotropic fixed point (black point) is at $\lambda = \lambda' = 1/(2N\rho_0)$ and is stable. The red fixed point is the isotropic fixed point of the SO$(M-1)$ model and is unstable and anisotropic in terms of M flavors. (b) Channel anisotropy with the case $N_1 = N_2$ shown. The isotropic fixed point (black point) is at $\lambda_1 = \lambda_2 = 1/2[(N_1 + N_2)\rho_0]$, which is unstable. Depending on which of λ_1 and λ_2 is larger, the stable fixed point is the purple $[\lambda_1 = 1/(2N_1\rho_0), \lambda_2 = 0]$ or the pink $[\lambda_1 = 0, \lambda_2 = 1/(2N_2\rho_0)]$ one.

$1/(2N_i\rho_0)$. The isotropic fixed point $\lambda_1 = \lambda_2 = 1/[2(N_1 + N_2)\rho_0]$ is unstable.

Conclusions.—We generalized the topological Kondo interaction into its $N \geq 2$-channel version by adding new sets of floating leads connected to the Majorana island (see Fig. 1). Consequently, we analyzed the two-channel case for its impurity entropy [Eq. (3)] and conductance [Eq. (2)]. The former indicates an emergent Fibonacci anyon, beyond the single-channel model. Another departure from the single-channel model is the NFL correction to conductance, which is of first order in the irrelevant operator, see below Eq. (8). The introduced multichannel generalization allowed us to develop a convergent large-N perturbation theory. Under the large-N limit, we found that the multichannel topological Kondo model has a stable fixed point at weak coupling. By using perturbative RG, we were able to solve for the running coupling constant, giving us the full crossover from the free fixed point to the intermediate one, see Eq. (7) and Fig. 2. We also considered the flavor and channel anisotropies in the large-N limit [see Fig. 3, Supplemental Material [69], and Eq. (11)], finding that the flavor anisotropy is irrelevant, while the channel anisotropy is relevant. Our Letter motivates the further study into the exotic physics found in multichannel Kondo models that are beyond conventional, SU(2)-symmetric, spin systems.

We thank Sergei Khlebnikov and Elio König for valuable discussions. This work was initiated at the Aspen Center for Physics, which is supported by National Science Foundation Grant No. PHY-1607611. Y. O. acknowledges support by the European Union's Horizon 2020 research and innovation program (Grant Agreement LEGOTOP No. 788715), the DFG (CRC/Transregio 183, EI 519/7-1), ISF Quantum Science and Technology (2074/19), the BSF, and NSF (2018643). This material is based upon work supported by the U.S. Department of Energy, Office of Science, National Quantum Information Science Research Centers, Quantum Science Center.

[1] J. Kondo, Resistance minimum in dilute magnetic alloys, Prog. Theor. Phys. **32**, 37 (1964).
[2] P. Nozieres and A. Blandin, Kondo effect in real metals, J. Phys. **41**, 193 (1980).
[3] M. Pustilnik and L. Glazman, Kondo effect in quantum dots, J. Phys. Condens. Matter **16**, R513 (2004).
[4] W. Pouse, L. Peeters, C. L. Hsueh, U. Gennser, A. Cavanna, M. A. Kastner, A. K. Mitchell, and D. Goldhaber-Gordon, Quantum simulation of an exotic quantum critical point in a two-site charge Kondo circuit, arXiv:2108.12691.
[5] I. Affleck, Conformal field theory approach to the Kondo effect, Acta Phys. Pol. B **26**, 1869 (1995), https://www.actaphys.uj.edu.pl/index_n.php?I=R&V=26&N=12#1869.
[6] D. L. C. A. Zawadowski, Exotic Kondo effects in metals: Magnetic ions in a crystalline electric field and tunnelling centres, Adv. Phys. **47**, 599 (1998).
[7] R. M. Potok, I. G. Rau, H. Shtrikman, Y. Oreg, and D. Goldhaber-Gordon, Observation of the two-channel Kondo effect, Nature (London) **446**, 167 (2007).
[8] A. J. Keller, L. Peeters, C. P. Moca, I. Weymann, D. Mahalu, V. Umansky, G. Zaránd, and D. Goldhaber-Gordon, Universal Fermi liquid crossover and quantum criticality in a mesoscopic system, Nature (London) **526**, 237 (2015).
[9] Z. Iftikhar, S. Jezouin, A. Anthore, U. Gennser, F. D. Parmentier, A. Cavanna, and F. Pierre, Two-channel Kondo effect and renormalization flow with macroscopic quantum charge states, Nature (London) **526**, 233 (2015).
[10] Z. Iftikhar, A. Anthore, A. K. Mitchell, F. D. Parmentier, U. Gennser, A. Ouerghi, A. Cavanna, C. Mora, P. Simon, and F. Pierre, Tunable quantum criticality and super-ballistic transport in a "charge" Kondo circuit, Science **360**, 1315 (2018).
[11] P. L. S. Lopes, I. Affleck, and E. Sela, Anyons in multichannel Kondo systems, Phys. Rev. B **101**, 085141 (2020).
[12] Y. Komijani, Isolating Kondo anyons for topological quantum computation, Phys. Rev. B **101**, 235131 (2020).
[13] D. Gabay, C. Han, P. L. S. Lopes, I. Affleck, and E. Sela, Multi-impurity chiral Kondo model: Correlation functions and anyon fusion rules, Phys. Rev. B **105**, 035151 (2022).
[14] M. Lotem, E. Sela, and M. Goldstein, Manipulating Non-Abelian Anyons in a Chiral Multichannel Kondo Model, Phys. Rev. Lett. **129**, 227703 (2022).
[15] V. J. Emery and S. Kivelson, Mapping of the two-channel Kondo problem to a resonant-level model, Phys. Rev. B **46**, 10812 (1992).
[16] A. M. Sengupta and A. Georges, Emery-Kivelson solution of the two-channel Kondo problem, Phys. Rev. B **49**, 10020 (1994).
[17] J. Gan, N. Andrei, and P. Coleman, Perturbative Approach to the Non-Fermi-Liquid Fixed Point of the Overscreened Kondo Problem, Phys. Rev. Lett. **70**, 686 (1993).

[18] A. Furusaki and K. A. Matveev, Coulomb Blockade Oscillations of Conductance in the Regime of Strong Tunneling, Phys. Rev. Lett. **75**, 709 (1995).
[19] P. Coleman, L. B. Ioffe, and A. M. Tsvelik, Simple formulation of the two-channel Kondo model, Phys. Rev. B **52**, 6611 (1995).
[20] A. V. Rozhkov, Impurity entropy for the two-channel Kondo model, Int. J. Mod. Phys. B **12**, 3457 (1998).
[21] T. Kimura, ABCD of Kondo Effect, J. Phys. Soc. Jpn. **90**, 024708 (2021).
[22] C. Han, Z. Iftikhar, Y. Kleeorin, A. Anthore, F. Pierre, Y. Meir, A. K. Mitchell, and E. Sela, Fractional Entropy of Multichannel Kondo Systems from Conductance-Charge Relations, Phys. Rev. Lett. **128**, 146803 (2022).
[23] I. Affleck and A. W. W. Ludwig, Universal Noninteger "Ground-State Degeneracy" in Critical Quantum Systems, Phys. Rev. Lett. **67**, 161 (1991).
[24] I. Affleck, A current algebra approach to the Kondo effect, Nucl. Phys. **B336**, 517 (1990).
[25] I. Affleck and A. W. Ludwig, The Kondo effect, conformal field theory and fusion rules, Nucl. Phys. **B352**, 849 (1991).
[26] I. Affleck and A. W. Ludwig, Critical theory of overscreened Kondo fixed points, Nucl. Phys. **B360**, 641 (1991).
[27] I. Affleck and A. W. W. Ludwig, Exact conformal-field-theory results on the multichannel Kondo effect: Single-fermion Green's function, self-energy, and resistivity, Phys. Rev. B **48**, 7297 (1993).
[28] A. W. Ludwig and I. Affleck, Exact conformal-field-theory results on the multi-channel Kondo effect: Asymptotic three-dimensional space-and time-dependent multi-point and many-particle Green's functions, Nucl. Phys. **B428**, 545 (1994).
[29] A. W. W. Ludwig and I. Affleck, Exact, Asymptotic, Three-Dimensional, Space- and Time-Dependent, Green's Functions in the Multichannel Kondo Effect, Phys. Rev. Lett. **67**, 3160 (1991).
[30] O. Parcollet, A. Georges, G. Kotliar, and A. Sengupta, Overscreened multichannel SU(N) Kondo model: Large-N solution and conformal field theory, Phys. Rev. B **58**, 3794 (1998).
[31] H. Yi, Resonant tunneling and the multichannel Kondo problem: Quantum Brownian motion description, Phys. Rev. B **65**, 195101 (2002).
[32] H. Yi and C. L. Kane, Quantum Brownian motion in a periodic potential and the multichannel Kondo problem, Phys. Rev. B **57**, R5579 (1998).
[33] A. M. Sengupta and Y. B. Kim, Overscreened single-channel Kondo problem, Phys. Rev. B **54**, 14918 (1996).
[34] N. Andrei and C. Destri, Solution of the Multichannel Kondo Problem, Phys. Rev. Lett. **52**, 364 (1984).
[35] A. M. Tsvelick and P. B. Wiegmann, Exact solution of the multichannel Kondo problem, scaling, and integrability, J. Stat. Phys. **38**, 125 (1985).
[36] J. Gan, On the multichannel Kondo model, J. Phys. Condens. Matter **6**, 4547 (1994).
[37] A. Holzner, I. P. McCulloch, U. Schollwöck, J. von Delft, and F. Heidrich-Meisner, Kondo screening cloud in the single-impurity Anderson model: A density matrix renormalization group study, Phys. Rev. B **80**, 205114 (2009).
[38] J. Martinek, L. Borda, Y. Utsumi, J. König, J. von Delft, D. Ralph, G. Schön, and S. Maekawa, Kondo effect in single-molecule spintronic devices, J. Magn. Magn. Mater. **310**, e343 (2007).
[39] C. P. Moca, A. Alex, J. von Delft, and G. Zaránd, Su(3) Anderson impurity model: A numerical renormalization group approach exploiting non-Abelian symmetries, Phys. Rev. B **86**, 195128 (2012).
[40] C. J. Lindner, F. B. Kugler, H. Schoeller, and J. von Delft, Flavor fluctuations in three-level quantum dots: Generic SU(3) Kondo fixed point in equilibrium and non-Kondo fixed points in nonequilibrium, Phys. Rev. B **97**, 235450 (2018).
[41] B. Béri and N. R. Cooper, Topological Kondo Effect with Majorana Fermions, Phys. Rev. Lett. **109**, 156803 (2012).
[42] B. Béri, Majorana-Klein Hybridization in Topological Superconductor Junctions, Phys. Rev. Lett. **110**, 216803 (2013).
[43] See also Refs. [44,45] for SO(5) Kondo model without Majoranas.
[44] A. K. Mitchell, A. Liberman, E. Sela, and I. Affleck, SO(5) Non-Fermi Liquid in a Coulomb Box Device, Phys. Rev. Lett. **126**, 147702 (2021).
[45] A. Liberman, A. K. Mitchell, I. Affleck, and E. Sela, SO(5) critical point in a spin-flavor Kondo device: Bosonization and refermionization solution, Phys. Rev. B **103**, 195131 (2021).
[46] Since we consider normal metal leads, by "channel" we mean a channel of itinerant complex fermions, equivalent to two Majorana fermion channels [47].
[47] A. Tsvelik, Topological Kondo effect in star junctions of Ising magnetic chains: Exact solution, New J. Phys. **16**, 033003 (2014).
[48] A. Altland, B. Béri, R. Egger, and A. M. Tsvelik, Bethe ansatz solution of the topological Kondo model, J. Phys. A **47**, 265001 (2014).
[49] L. Herviou, K. Le Hur, and C. Mora, Many-terminal Majorana island: From topological to multichannel Kondo model, Phys. Rev. B **94**, 235102 (2016).
[50] K. Michaeli, L. A. Landau, E. Sela, and L. Fu, Electron teleportation and statistical transmutation in multiterminal Majorana islands, Phys. Rev. B **96**, 205403 (2017).
[51] M. Papaj, Z. Zhu, and L. Fu, Multichannel charge Kondo effect and non-Fermi-liquid fixed points in conventional and topological superconductor islands, Phys. Rev. B **99**, 014512 (2019).
[52] J. I. Väyrynen, A. E. Feiguin, and R. M. Lutchyn, Signatures of topological ground state degeneracy in Majorana islands, Phys. Rev. Res. **2**, 043228 (2020).
[53] K. Snizhko, F. Buccheri, R. Egger, and Y. Gefen, Parafermionic generalization of the topological Kondo effect, Phys. Rev. B **97**, 235139 (2018).
[54] M. R. Galpin, A. K. Mitchell, J. Temaismithi, D. E. Logan, B. Béri, and N. R. Cooper, Conductance fingerprint of Majorana fermions in the topological Kondo effect, Phys. Rev. B **89**, 045143 (2014).
[55] E. Eriksson, C. Mora, A. Zazunov, and R. Egger, Non-Fermi-Liquid Manifold in a Majorana Device, Phys. Rev. Lett. **113**, 076404 (2014).

[56] O. Kashuba and C. Timm, Topological Kondo Effect in Transport through a Superconducting Wire with Multiple Majorana End States, Phys. Rev. Lett. **114**, 116801 (2015).
[57] F. Buccheri, G. D. Bruce, A. Trombettoni, D. Cassettari, H. Babujian, V. E. Korepin, and P. Sodano, Holographic optical traps for atom-based topological Kondo devices, New J. Phys. **18**, 075012 (2016).
[58] B. Béri, Exact Nonequilibrium Transport in the Topological Kondo Effect, Phys. Rev. Lett. **119**, 027701 (2017).
[59] F. Buccheri, H. Babujian, V. E. Korepin, P. Sodano, and A. Trombettoni, Thermodynamics of the topological Kondo model, Nucl. Phys. **B896**, 52 (2015).
[60] D. Liu, Z. Cao, X. Liu, H. Zhang, and D. E. Liu, Topological Kondo device for distinguishing quasi-Majorana and Majorana signatures, Phys. Rev. B **104**, 205125 (2021).
[61] Y. Kuramoto, Perturbative renormalization of multi-channel Kondo-type models, Eur. Phys. J. B **5**, 457 (1998).
[62] Y. Oreg and D. Goldhaber-Gordon, Non-Fermi-liquid in a modified single electron transistor, arXiv:cond-mat/0203302.
[63] Y. Oreg and D. Goldhaber-Gordon, Two-Channel Kondo Effect in a Modified Single Electron Transistor, Phys. Rev. Lett. **90**, 136602 (2003).
[64] N. Hartman, C. Olsen, S. Lüscher, M. Samani, S. Fallahi, G. C. Gardner, M. Manfra, and J. Folk, Direct entropy measurement in a mesoscopic quantum system, Nat. Phys. **14**, 1083 (2018).
[65] E. Sela, Y. Oreg, S. Plugge, N. Hartman, S. Lüscher, and J. Folk, Detecting the Universal Fractional Entropy of Majorana Zero Modes, Phys. Rev. Lett. **123**, 147702 (2019).
[66] T. Child, O. Sheekey, S. Lüscher, S. Fallahi, G. C. Gardner, M. Manfra, A. Mitchell, E. Sela, Y. Kleeorin, Y. Meir, and J. Folk, Entropy Measurement of a Strongly Coupled Quantum Dot, Phys. Rev. Lett. **129**, 227702 (2021).
[67] E. Pyurbeeva, J. A. Mol, and P. Gehring, Electronic measurements of entropy in meso- and nanoscale systems, Chem. Phys. Rev. **3**, 041308 (2022).
[68] T. Child, O. Sheekey, S. Lüscher, S. Fallahi, G. C. Gardner, M. Manfra, and J. Folk, A robust protocol for entropy measurement in mesoscopic circuits, Entropy **24**, 417 (2022).
[69] See Supplemental Materials at http://link.aps.org/supplemental/10.1103/PhysRevLett.130.066302 for additional details, including calculation of large-N fixed point conductance and impurity entropy.
[70] T. Kimura and S. Ozaki, Fermi/non-Fermi mixing in SU(N) Kondo effect, J. Phys. Soc. Jpn. **86**, 084703 (2017).
[71] J. Alicea and P. Fendley, Topological phases with parafermions: Theory and blueprints, Annu. Rev. Condens. Matter Phys. **7**, 119 (2016).
[72] P. W. Anderson, A poor man's derivation of scaling laws for the Kondo problem, J. Phys. C **3**, 2436 (1970).
[73] E. Kogan and Z. Shi, Poor man's scaling: XYZ Coqblin–Schrieffer model revisited, J. Stat. Mech. (2021) 033101.
[74] I. Affleck, A. W. W. Ludwig, H.-B. Pang, and D. L. Cox, Relevance of anisotropy in the multichannel Kondo effect: Comparison of conformal field theory and numerical renormalization-group results, Phys. Rev. B **45**, 7918 (1992).
[75] The leading irrelevant operator is the first descendent of the adjoint primary operator.
[76] L.-Y. Hung, Y.-S. Wu, and Y. Zhou, Linking entanglement and discrete anomaly, J. High Energy Phys. 05 (2018) 008.
[77] P. Francesco, P. Mathieu, and D. Sénéchal, *Conformal Field Theory* (Springer Science & Business Media, New York, 2012).
[78] D. Friedan and A. Konechny, Boundary Entropy of One-Dimensional Quantum Systems at Low Temperature, Phys. Rev. Lett. **93**, 030402 (2004).
[79] N. Andrei and A. Jerez, Fermi- and Non-Fermi-Liquid Behavior in the Anisotropic Multichannel Kondo Model: Bethe Ansatz Solution, Phys. Rev. Lett. **74**, 4507 (1995).